



**HAL**  
open science

## Micromechanical properties of the healthy canine medial meniscus

Véronique Livet, Romain Rieger, Éric Viguié, Thibaut Cachon, C. Boulocher

► **To cite this version:**

Véronique Livet, Romain Rieger, Éric Viguié, Thibaut Cachon, C. Boulocher. Micromechanical properties of the healthy canine medial meniscus. *Research in Veterinary Science*, 2022, 147, pp.20-27. 10.1016/j.rvsc.2022.03.018 . hal-03674001

**HAL Id: hal-03674001**

**<https://hal.science/hal-03674001>**

Submitted on 27 Jun 2022

**HAL** is a multi-disciplinary open access archive for the deposit and dissemination of scientific research documents, whether they are published or not. The documents may come from teaching and research institutions in France or abroad, or from public or private research centers.

L'archive ouverte pluridisciplinaire **HAL**, est destinée au dépôt et à la diffusion de documents scientifiques de niveau recherche, publiés ou non, émanant des établissements d'enseignement et de recherche français ou étrangers, des laboratoires publics ou privés.

1 **Original Article**

2  
3  
4 **Micromechanical properties of the healthy canine medial meniscus.**

5  
6 Véronique Livet <sup>a,b,#</sup>, Romain Rieger <sup>a,c,#,\*</sup>, Éric Viguiier <sup>a,b</sup>, Thibaut Cachon <sup>a,b</sup>, Caroline  
7 Boulocher <sup>a,d</sup>

8  
9 <sup>a</sup> *Université de Lyon, VetAgro Sup, UPSP ICE 2021.A104, 69280 Marcy l'Étoile, France*

10 <sup>b</sup> *Surgery Unit of VetAgro Sup, VetAgro Sup, 69280 Marcy l'Étoile, France*

11 <sup>c</sup> *Université de Lyon, Ecole Centrale de Lyon, 69134 Ecully Cedex, France*

12 <sup>d</sup> *Institut Polytechnique UniLaSalle, Campus de Rouen, 76000 Rouen, France*

13  
14  
15  
16 # These authors contributed equally to this work

17 \* Corresponding author.

18  
19 Romain Rieger  
20 Ecole Centrale de Lyon  
21 Department MSGMGC  
22 UPSP ICE 2021.A104 VetAgro Sup  
23 36 avenue Guy de Collongue  
24 Bâtiment G8  
25 69134 Ecully Cedex  
26  
27 [romain.rieger@ec-lyon.fr](mailto:romain.rieger@ec-lyon.fr)

28  
29

30 **Abstract**

31           Aims: Knowledge of the micromechanical characteristics of the menisci is required to  
32 better understand their role within the stifle joint, improve early diagnosis of meniscal lesions,  
33 and develop new treatment and/or replacement strategies. The aim of the study was to determine  
34 the mechanical properties of the healthy medial canine meniscus and to evaluate the effect of  
35 regional (caudal, central, and cranial) and circumference (axial and abaxial) locations on these  
36 properties.

37

38           Methods: To study the micromechanical properties of the medial menisci in healthy  
39 (Beagle) dogs, the influence of regional (caudal, central, and cranial) and circumference (axial  
40 and abaxial) locations were evaluated. Nanoindentation-relaxation tests were performed to  
41 characterize the local stiffness and the viscoelastic properties at each region and specific  
42 circumference. Linear interpolation onto the indentation points was performed to establish a  
43 map of the micromechanical property heterogeneities.

44

45           Results: The results indicate that the cranial region was significantly stiffer and less  
46 viscous than the central and caudal regions. Within the central region the inner part (axial) was  
47 significantly stiffer than the periphery (abaxial). Within the caudal region the inner part was  
48 significantly less viscous than the periphery.

49

50           Conclusion: Significant regional and radial variations were observed for both the  
51 stiffness and the viscoelastic properties. Moreover, a viscous behavior of the entire medial  
52 meniscus was observed (elastic fraction  $< 0.5$ ). These results deter the use of average elastic  
53 modulus to study the regional mechanical properties of healthy meniscus.

54 *Keywords:* Meniscus, nanoindentation-relaxation, viscoelasticity

55

## 56 **Introduction**

57           The stifle menisci are important contributors to joint function. They enhance  
58 congruence between the femoral condyles and tibial plateau, which increase the area of load  
59 distribution and reduce mechanical stresses in the joint (Makris et al., 2011). They provide joint  
60 lubrication (Clark et al., 1999), contribute to the stability of the stifle (Fox et al., 2015), assist  
61 proprioception, and coordinate muscle contraction (Messner and Gao, 1998). The stifle menisci  
62 also act as a primary passive restraint of cranial tibial translation (Pozzi et al., 2006).

63           Anatomically, the stifle menisci are two C-shaped fibrocartilages anchored within the femoro-  
64 tibial joint by ligamentous attachments to the tibia, the femur, and to each other (Bennett and  
65 May, 1991; Briggs, 2004).

66           Being better fixed and less mobile than the lateral meniscus, the medial meniscus is  
67 more prone to damage in case of translation of the tibia leading to a bucket-handle tear of the  
68 caudal horn of the medial meniscus (Casale and McCarthy, 2009; Case et al., 2008). Meniscal  
69 tears are usually associated with the rupture of the cranial cruciate ligament, one of the most  
70 frequent orthopedic conditions in this species (Witsberger et al., 2008). Only the abaxial 15-  
71 25% of the adult menisci is having a blood supply (Arnoczky and Warren, 1983), this vascular  
72 anisotropy limits the healing potential of meniscal tears in this location.

73           Structurally, menisci have a triangular cross-section with a thicker abaxial (outer) rim  
74 that tapers to a thin, almost translucent, axial (inner) edge. At the microscopic scale the  
75 anisotropy of collagen type I fibers organization induce regionally dependent dynamic  
76 mechanical properties (storage and loss modulus) as shown in human and bovine (Moyer et al.,  
77 2013; Murphy et al., 2019). The present study provides a quantified mapping of the viscoelastic  
78 behavior across and within the main load bearing regions in the healthy dog's stifle medial  
79 meniscus. Spatial mapping of the mechanical properties of small, thin and heterogeneous soft  
80 biological tissues have been commonly measured by nanoindentation techniques (Ebenstein et

81 al., 2004; Oyen, 2015). Nanoindentation is a contact mechanics experiment during which the  
82 full force–displacement–time response is monitored (Oyen, 2015). The local stiffness can be  
83 determined by nanoindentation (Moyer et al., 2012), the viscoelastic mechanical behavior can  
84 be determined by creep and relaxation-indentation tests (Moyer et al., 2013). Creep  
85 nanoindentation on cylindrical meniscal plugs has been performed on canine menisci (Noone  
86 et al., 2002; Sweigart et al., 2004). This approach presents an ill-posed problem so that a small  
87 error in the creep compliance function can lead to large errors in the relaxation modulus (Huang  
88 and Lu, 2006). Nanoindentation-relaxation tests on canine menisci has, to the best of our  
89 knowledge, not been used and is lacking.

90

91 The purposes of the study were to determine the mechanical properties of the healthy  
92 medial canine meniscus through nanoindentation-relaxation, to evaluate the effect of regional  
93 (caudal, central, and cranial) and circumference (axial and abaxial) locations. Our hypotheses  
94 were that there was i) a difference in stiffness between the regions ii) and within the  
95 circumferences of the menisci. The results of this study could help to track and understand the  
96 localized onset of the mechanical properties degradation of the medial meniscal tears.

97

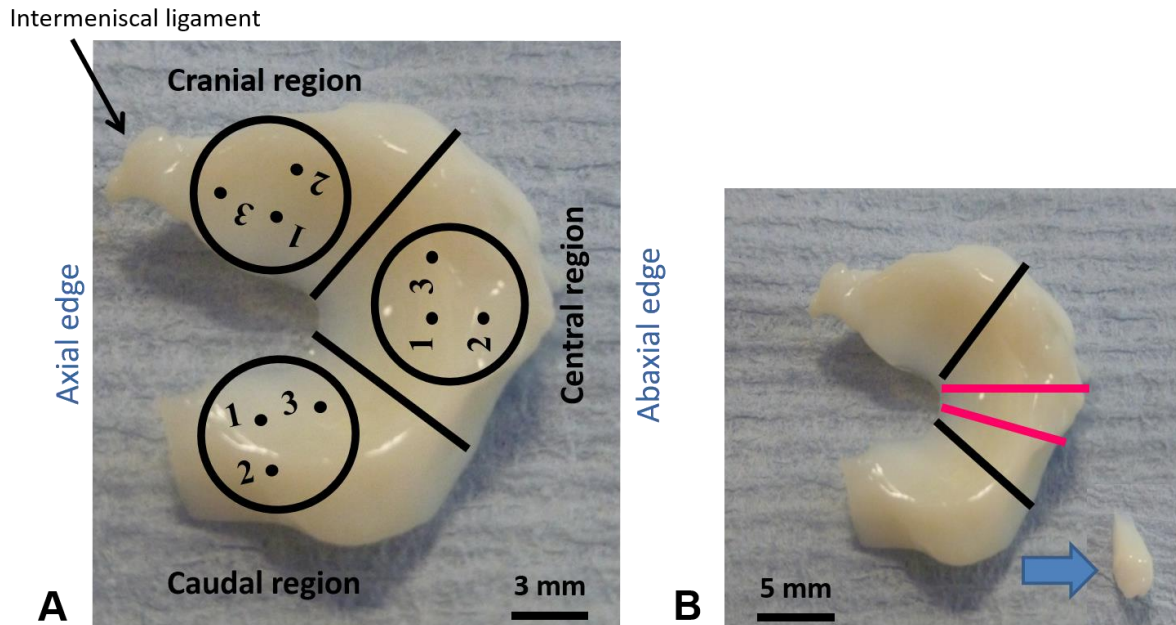
98

## 99 **Materials and methods**

### 100 *Sample preparation*

101 Six healthy research dogs were selected from a colony of purpose-bred Beagles being  
102 euthanized as an endpoint in a study unrelated to the present one. Each dog was considered  
103 “healthy” based on results of a physical examination, orthopaedic examination and stifle  
104 radiographs, all performed by board-certified veterinary surgeons on the day of the procedure.  
105 The study follows the ARRIVE guidelines, the checklist is provided in the Supplementary  
106 Material. All dogs were spayed females aged of about one-year-old with a mean body weight

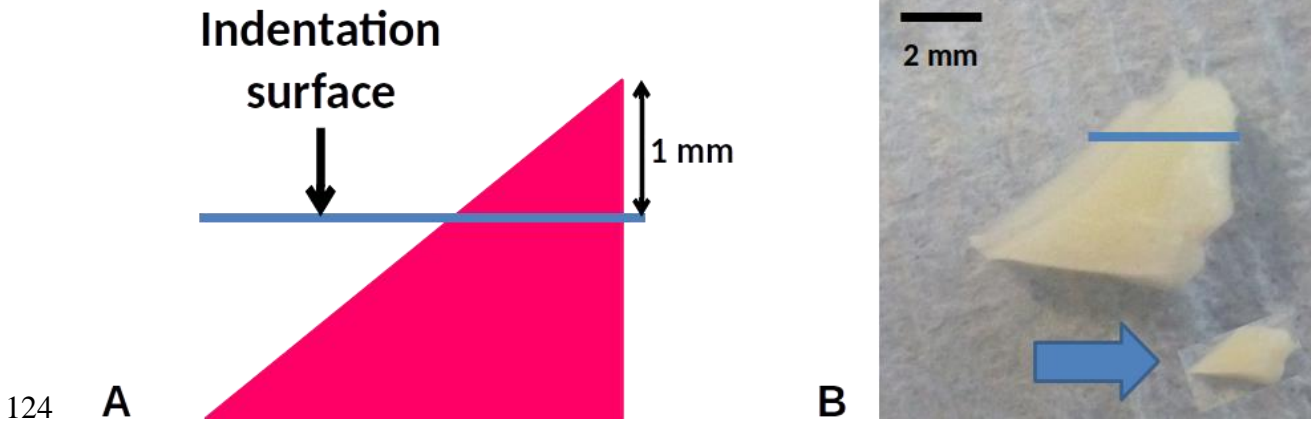
107 of  $10.5 \pm 0.6$  kg (range from 9.6 to 11 kg). Menisci were removed from the left stifle of the  
108 dogs in the hours ( $< 4$  hours) following euthanasia by transecting the cruciate and collateral  
109 ligaments, all meniscal attachments, and the joint capsule. Left medial menisci were placed in  
110 gauze moistened with saline and deposited in biopsy jars stored at  $-20^{\circ}\text{C}$ .



111

112 Fig. 1. (A) Optical image of the femoral surface of a healthy medial meniscus (left stifle),  
113 localization of the three studied regions (cranial, central, caudal) and of the three studied points  
114 within each region (points 1 and 3 are on the same axial circumference and point 2 is more  
115 peripheral). (B) Optical image of the experimental procedure showing a slice of 2 mm in width  
116 cut with a scalpel through the cross-section. The arrow shows the slice once cut.  
117

118 Before dissection and testing, menisci were placed in the refrigerator at  $+4^{\circ}\text{C}$  for 24  
119 hours (Levillain et al., 2015). Each meniscus was measured and trisected into cranial, central,  
120 and caudal regions for regional comparison. Two millimeters wide sections were cut through  
121 the cross-section, in the middle of each region (Fig. 1) and each sample was cut parallel to the  
122 tibial meniscal surface at approximately 1 mm high from this surface so that the indenter tip  
123 could be perpendicular to the second cut area (Fig. 2) (Levillain et al., 2015).



124 **A** **B**

125 Fig. 2. The blue line represents the cutting plane horizontal to the distal (tibial) surface. The  
 126 indentation direction was perpendicular to the cutting plane. (A) Representation of the height  
 127 of the cutting plane (1mm from the highest height). (B) Optical image of a 2 mm wide section,  
 128 the arrow shows the tip of the meniscus once cut and the flatness of the section.  
 129

130 *Gross evaluation*

131 Menisci length, width and maximal height were measured. The measures were repeated  
 132 three times by the same operator. Pictures were taken for each meniscus for record.

133

134 *Nanoindentation*

135 Nanoindentation was performed using a nanoindenter with a spherical sapphire tip, with  
 136 a radius of curvature  $R = 0.479$  mm (Nano Indenter G200, Agilent Technologies, Science Tec).  
 137 The opposite face of indentation was glued on a petri dish. Samples were covered with saline  
 138 so that menisci stayed correctly hydrated during all testing. The temperature was maintained at  
 139  $21^{\circ}\text{C}$  in the test-room. Nanoindentation was performed on the cranial, central, and caudal  
 140 regions in the deep zone of the menisci. For each three regions, nanoindentation tests were  
 141 carried out on three locations (thereafter named points) covering the maximal area of the  
 142 sample. Point 1 and point 3 were placed on the same axial circumference while point 2 was  
 143 placed more on the periphery (Fig. 1A). Each point was spaced at least  $350\ \mu\text{m}$  apart from the  
 144 others to avoid effects from subsequent indents. Each test was repeated three times for each

145 point. Then calculated parameters (elastic and viscoelastic models) were averaged for each  
146 indentation point.

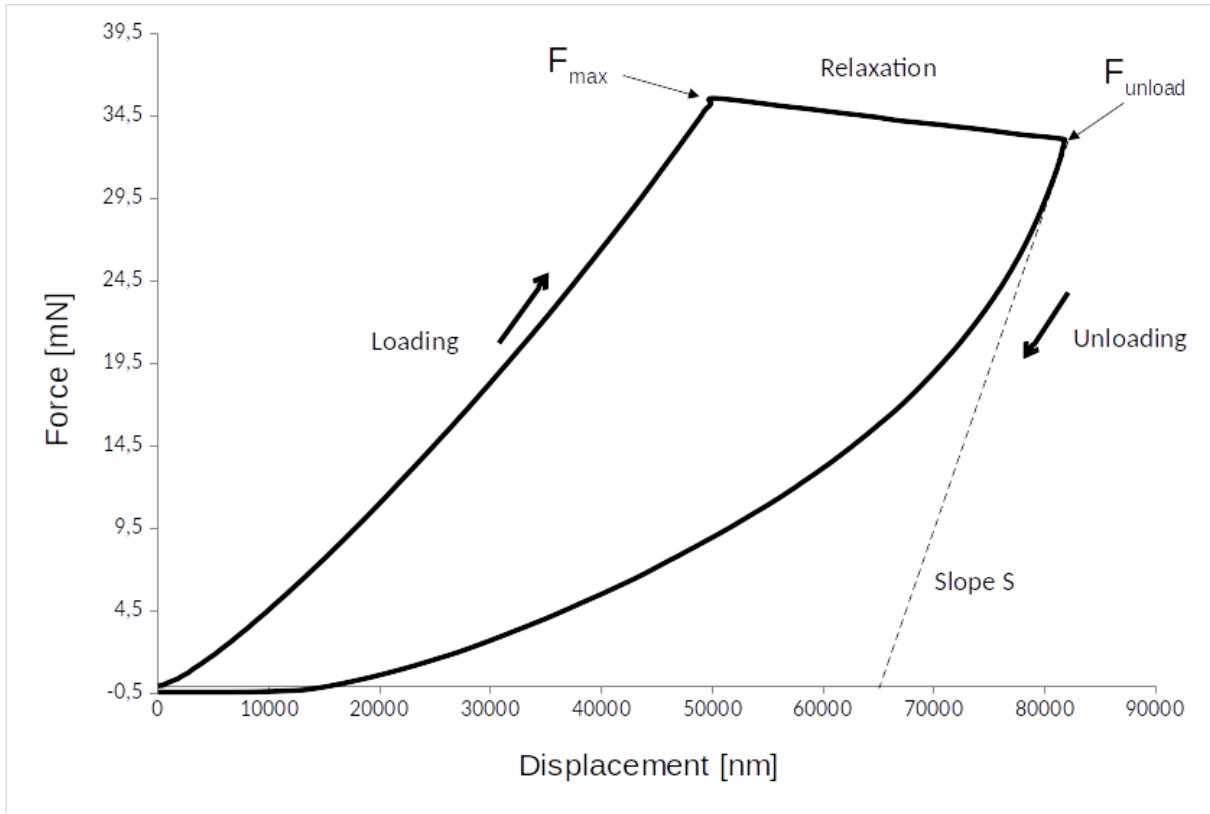
147

148 To ensure reliability of the measurement, a reference material (rubber) was first indented  
149 before each series of tests on a given meniscus sample. The tip of the indenter was placed 20  
150  $\mu\text{m}$  above the cut surface of the meniscus. During the loading path, a constant displacement rate  
151 of 10  $\mu\text{m/s}$  was imposed until a penetration of 50  $\mu\text{m}$ . The indenter displacement was  
152 maintained for 400 seconds (until equilibrium was reached), to avoid a discontinuity of the  
153 force when unloading due to the viscoelasticity of the meniscus. Finally, the unloading path  
154 was carried out at a displacement rate of 0.5  $\mu\text{m/s}$ . These testing parameters were chosen based  
155 on preliminary tests and aimed to limit surface penetration. Overall, 27 tests were performed  
156 on each meniscus: 3 indentation measurements per points x 3 points per region x 3 regions,  
157 leading to 162 tests in total (6 samples).

158

### 159 *Elastic model*

160 On the resultant force-displacement curve, the maximal force ( $F_{max}$ ) was measured when  
161 the displacement reached 50  $\mu\text{m}$  and was extracted from each test (Fig. 3). After the relaxation  
162 (400 seconds), the force obtained at the start of the unloading path ( $F_{unload}$ ) was also extracted  
163 from each test. The reduced modulus  $E_r$  at the start of the unloading path was computed by the  
164 Hertz theory (Oliver and Pharr, 1992) for each point, as:  $E_r = \frac{S\sqrt{\pi}}{2\sqrt{A}} = \frac{S}{2\sqrt{\delta R}}$ , where the slope  $S =$   
165  $\left. \frac{dF}{d\delta} \right|_{F_{unload}}$  is the contact stiffness, A is the Hertz contact area,  $\delta$  is the maximal penetration, and  
166 R is the radius of the indenter. The maximal penetration corresponded to the end of the  
167 relaxation time and the beginning of the unloading path. This displacement corresponded to  
168  $F_{unload}$ . The contact stiffness corresponded to the linear portion of the unloading phase slope  
169 between  $F_{unload}$  and 80% of that force.



170

171 Fig. 3. Typical force - displacement curve obtained by nanoindentation-relaxation experiment  
 172 of the canine meniscus.

173

174 *Viscoelastic model*

175 The instantaneous modulus ( $E_{ins}$ ), the equilibrium modulus ( $E_{eq}$ ) and the elastic fraction

176 ( $f = \frac{E_{eq}}{E_{ins}}$ ) were determined from the resultant force-time data using the Hertzian contact for a

177 linear viscoelastic material model. Briefly, the resultant force-time for a spherical indenter can

178 be expressed as :  $F(t) = \frac{8\sqrt{R}}{3(1-\nu)} \int_0^t G(t-s) \frac{dh(s)^{3/2}}{ds} ds$  where  $F$  is the force,  $h$  is the penetration of the

179 indenter,  $\nu = 0.49$  is the Poisson coefficient, assuming incompressibility of the menisci and for

180 numerical considerations (Danso et al., 2015), and  $R = 0.479mm$  is the radius of the indenter.

181 The shear relaxation modulus  $G(t)$  was described using Prony series with four branches

182 (Levillain et al., 2017) described as :  $G(t) = G_0 + \sum_{i=1}^4 G_i e^{(-t/\tau_i)}$  where  $G_0$  and  $G_i$  are the shear

183 relaxation coefficients and  $\tau_i$  is the retardation time. The instantaneous, the equilibrium modulus

184 and the elastic fraction ( $E_{ins}$ ,  $E_{eq}$  and  $f$  respectively) were computed according to :  $E_{ins} =$

185  $2(1 + \nu)(G_0 + \sum_{i=1}^4 G_i)$  ,  $E_{eq} = 2(1 + \nu)G_0$  and  $f = \frac{E_{eq}}{E_{ins}}$ . The elastic fraction describes the  
186 elastic/viscous behaviour of the material. A perfectly elastic behavior corresponds to  $f = 1$   
187 whereas a perfectly viscous behavior corresponds to  $f = 0$ . Details of the equation solving are  
188 provided in the appendix of Levillain et al., 2017.

189

### 190 *Statistical analysis*

191 Statistical analysis was performed using R (R Foundation for Statistical Computing,  
192 Vienna, Austria). First, a Shapiro-Wilk test was used for each point to define if parametric or  
193 non-parametric tests need to be performed. Since non-parametric tests were needed, a Kruskal-  
194 Wallis test was used for all analyses (level of significance  $\alpha = 0.05$ ). Pairwise Wilcoxon rank  
195 sum tests were used as a post hoc test ( $\alpha = 0.05$ ).

196

197 To assess mechanical heterogeneity, the analysis unit was the location of an indentation  
198 point. Two studies were conducted: *i*) the effect of regional location by comparisons between  
199 cranial, central, and caudal regions. For each indentation point, each group (cranial, central, and  
200 caudal regions) consisted in 18 independent observations (6 menisci x 3 nanoindentation tests  
201 per point in the corresponded region); *ii*) the effect of circumference by comparisons between  
202 point 1, point 2 and point 3. For each region, each group (point 1, point 2, point 3) consisted in  
203 18 independent observations (6 menisci x 3 nanoindentation tests per point per region). For  
204 each study, the degree of freedom of the analysis of variance E is computed by the following  
205 formulae:  $E = \text{Total independent observations per study} - \text{Total number of groups}$ , which leads  
206 to  $E = 18 - 3 = 15 > 10$ . Since E should lie between 10 and 20 (Charan and Kantharia, 2013),  
207 the sample size in this study should be adequate to assess statistical significance.

208

### 209 *Heterogeneity mapping*

210 Mechanical heterogeneity was represented by linear interpolation between the known  
211 mean values of the nine indentation points and presumed fixed border values named  $\bar{g}$ . The  
212 mechanical property (reduced modulus  $E_r$  or elastic fraction  $f$  of each indentation point was  
213 denoted as  $g$ . The mean value  $\bar{g}_i^k$  across all samples was defined by:  $\bar{g}_i^k = \frac{\sum_{j=1}^n g_i^k}{n}$  where  $i = 1,3$   
214 represents the  $i^{\text{th}}$  indentation point,  $k = 1,3$  represents the  $k^{\text{th}}$  region (cranial, central, caudal),  
215 and  $j = 1,6$  represents the  $j^{\text{th}}$  sample. Each pixel forming the border of the meniscus was  
216 represented by the same mean value across the whole sample defined by:  $\bar{g} = \frac{\sum_{i=1}^n \sum_{j=1}^n g_i^j}{n}$  where  
217  $i = 1,9$  represents the  $i^{\text{th}}$  indentation point, and  $j = 1,6$  represents the  $j^{\text{th}}$  sample.

218

## 219 **Results**

### 220 *Global evaluation*

221 The mean value of the left medial meniscus's length was  $14.3 \pm 0.8$  mm, the mean  
222 width  $6 \pm 2.2$  mm and the mean height  $4.2 \pm 0.8$  mm. No difference in terms of inner/outer  
223 thickness and length were observed between left and right menisci.

224

225 The reduced modulus and the elastic fraction showed significant differences  
226 depending on the region and on the circumference as described below. In all regions and  
227 circumferences, the elastic fraction was strictly inferior to 0.5, which denotes an overall viscous  
228 behavior rather than an elastic one of the healthy canine menisci. All data (mean  $\pm$  sd of the 3  
229 nanoindentation tests for each point) are detailed in Table 1.

230

231 **Table 1**

232 Summary table of: (A) the maximal force  $F_{\max}$ ; (B) the force obtained at the start of the unloading path  $F_{\text{unload}}$ ; (C) the reduced modulus  $E_r$ ; (D)  
 233 the instantaneous modulus,  $E_{\text{ins}}$ ; (E) the equilibrium modulus  $E_{\text{eq}}$  and the elastic fraction  $f$ , presented as mean +/- SD for each three points of each  
 234 three regions for each six samples.

	<b>Caudal point1</b>	<b>Caudal point2</b>	<b>Caudal point3</b>	<b>Central point1</b>	<b>Central point2</b>	<b>Central point3</b>	<b>Cranial point1</b>	<b>Cranial point2</b>	<b>Cranial point3</b>
<b>Fmax [mN]</b>									
<b>Sample 1</b>	7.47±1.23	23.07±0.4	15.17±0.15	14.07±0.81	10.57±0.06	10.47±0.42	38.07±2.27	56.1±0.35	41.53±1.31
<b>Sample 2</b>	12.1±0.2	7.7±0.17	11.4±0.3	16.3±0.17	5.43±0.31	14.47±0.32	47.1±1.08	57.97±0.87	70.77±1.19
<b>Sample 3</b>	3.73±0.12	3.27±0.06	4.57±0.15	13.93±0.25	8.8±0.1	10.5±0.1	9.23±0.61	4.23±0.12	3.67±0.47
<b>Sample 4</b>	61.53±2.01	30.23±3.17	38.13±1.15	26.6±0.36	10.17±0.71	28.03±0.32	43.57±1.22	35.67±0.06	47±0.1
<b>Sample 5</b>	16.13±0.15	6.7±0.26	14.63±0.15	5.93±0.15	3.9±0	6.33±0.47	47.93±1.65	67.4±1.13	40.73±1.72
<b>Sample 6</b>	6.63±0.31	4.33±0.06	7.17±0.12	6.83±0.31	4.47±0.25	5.67±0.25	47.83±0.81	45.27±1.62	38.8±0.9
<b>Funload [mN]</b>									
<b>Sample 1</b>	5.4±1.15	19.87±0.31	12.13±0.12	10.73±0.5	7.37±0.32	7.57±0.67	35.47±2.44	53.33±0.38	39.37±1.03
<b>Sample 2</b>	9.03±0.31	4.7±0.17	8.07±0.35	12.6±0.2	2.8±0.26	10.87±0.32	45.33±1.26	55.73±0.46	68.5±0.79
<b>Sample 3</b>	1.9±0.17	1.07±0.06	2.7±0.1	10.13±0.06	5.8±0.1	7±0.26	5.87±0.7	1.4±0	1.23±0.25
<b>Sample 4</b>	57.9±2.07	28.03±2.87	34.67±1.1	23.37±0.25	8.7±0.62	24.87±0.29	40.67±1.36	33.13±0.06	43.87±0.25
<b>Sample 5</b>	13.47±0.15	4.03±0.21	11.87±0.12	3.1±0.2	1.3±0	3.23±0.38	46.17±1.7	64.37±1.18	38.97±1.66
<b>Sample 6</b>	4.37±0.32	2.37±0.06	4.73±0.06	4.27±0.59	1.77±0.25	3.43±0.21	45.47±0.76	43.37±1.56	36.83±0.85
<b>Er [MPa]</b>									
<b>Sample 1</b>	1.12±0.24	2.87±0.02	2.17±0.09	1.69±0.02	1.61±0.05	1.38±0.05	4.92±0.17	7.44±0.25	4.66±0.15
<b>Sample 2</b>	1.54±0.03	0.88±0.01	1.46±0.12	2.62±0.01	0.58±0.03	2.41±0.02	7.44±0.16	7.93±0.11	8.58±0.2
<b>Sample 3</b>	0.32±0.01	0.17±0.02	0.44±0.02	1.65±0.03	1.03±0.01	1.15±0.02	1.74±0.1	0.21±0.06	0.25±0.01
<b>Sample 4</b>	7.78±0.17	6.42±0.16	6.2±0.16	3.29±0.05	2.71±0.17	3.39±0.03	4.19±0.22	4.14±0.16	5.14±0.18

<b>Sample 5</b>	2.63±0.08	0.91±0.02	2.46±0.05	0.75±0.04	0.2±0	0.84±0.02	10.87±0.49	8.64±0.14	8.37±0.05
<b>Sample 6</b>	0.62±0.03	0.31±0.01	0.87±0.01	0.94±0.02	0.34±0.09	0.79±0.03	5.79±0.03	6.89±0.15	5.89±0.11

**Eins [MPa]**

<b>Sample 1</b>	0.81±0.15	2.34±0.07	1.94±0.74	1.47±0.14	1.22±0.08	1.1±0.07	3.99±0.16	5.88±0.26	4.94±0.09
<b>Sample 2</b>	1.23±0.05	0.79±0.03	1.17±0.08	1.72±0.08	0.56±0.06	1.49±0.09	4.75±0.09	5.97±0.29	7.31±0.3
<b>Sample 3</b>	0.35±0.03	0.3±0.05	0.48±0.08	1.49±0.25	0.92±0.02	1.12±0.04	1.01±0.14	0.45±0.04	0.38±0.1
<b>Sample 4</b>	6.28±0.48	3.01±0.29	3.96±0.34	2.69±0.12	1.14±0.07	2.89±0.2	4.36±0.2	3.48±0.14	4.72±0.09
<b>Sample 5</b>	1.69±0.02	0.71±0.07	1.44±0.04	0.71±0.12	0.46±0	0.73±0.05	5.22±0.31	6.99±0.31	4.8±0.15
<b>Sample 6</b>	0.38±0.01	0.41±0.03	1.2±0.76	0.81±0.11	0.16±0.02	0.59±0.04	4.77±0.27	4.37±0.11	3.92±0.13

**Eeq [MPa]**

<b>Sample 1</b>	0.18±0.04	0.48±0.02	0.36±0.01	0.29±0.01	0.2±0.02	0.2±0.04	1.12±0.1	1.65±0.05	1.23±0.01
<b>Sample 2</b>	0.28±0.02	0.14±0	0.24±0.01	0.37±0.01	0.08±0.01	0.32±0.01	1.54±0.06	1.79±0.04	1.86±0.02
<b>Sample 3</b>	0.06±0.01	0.01±0.01	0.1±0	0.27±0.01	0.19±0	0.21±0.02	0.19±0.02	0.01±0.01	0.03±0
<b>Sample 4</b>	1.64±0.07	1.06±0.06	1.06±0.01	0.73±0.04	0.42±0.02	0.77±0.04	1.07±0.08	1.08±0.05	1.17±0.13
<b>Sample 5</b>	0.44±0.02	0.14±0	0.4±0.01	0.1±0.01	0.02±0	0.1±0.01	1.82±0.09	1.88±0.05	1.48±0.05
<b>Sample 6</b>	0.11±0.01	0.08±0	0.17±0.01	0.14±0.03	0.02±0.01	0.12±0.01	1.51±0.08	1.58±0.05	1.39±0.03

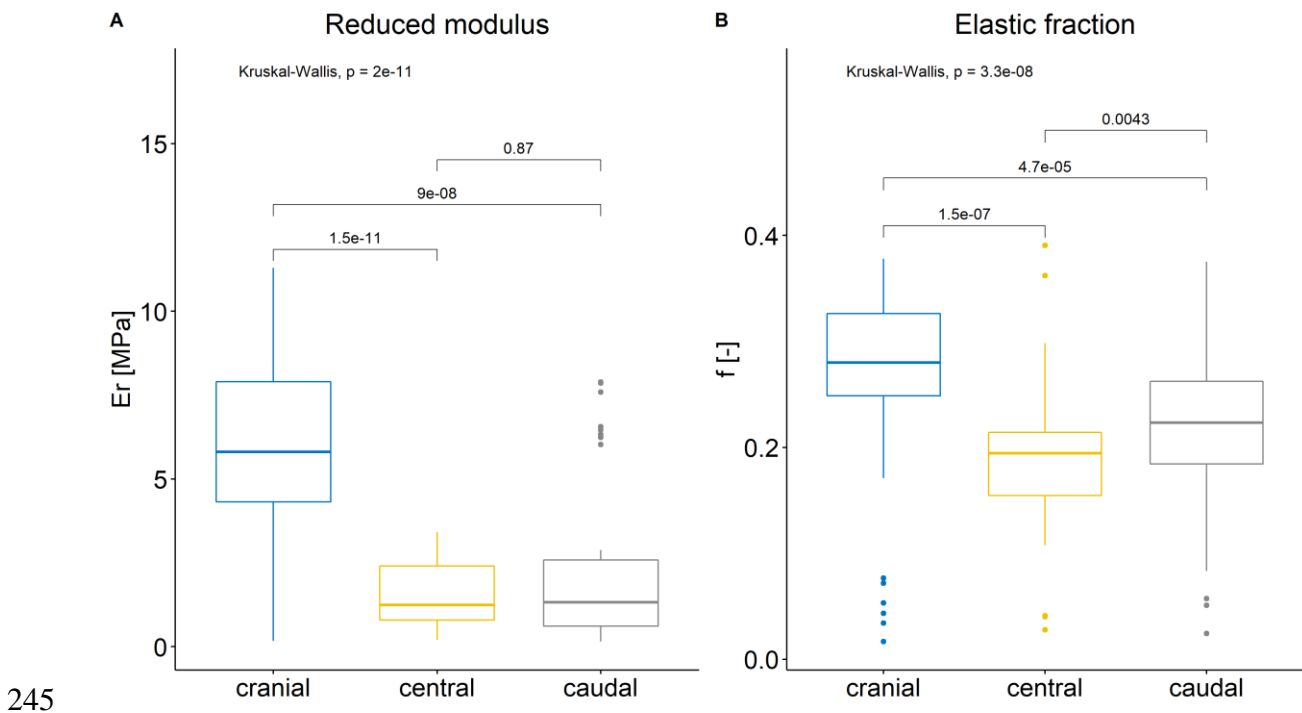
**f [-]**

<b>Sample 1</b>	0.22±0.01	0.21±0.01	0.2±0.07	0.2±0.01	0.17±0.01	0.18±0.03	0.28±0.02	0.28±0.02	0.25±0
<b>Sample 2</b>	0.23±0.01	0.18±0	0.2±0.01	0.21±0	0.14±0.02	0.22±0.01	0.32±0.01	0.3±0.02	0.25±0.01
<b>Sample 3</b>	0.17±0.02	0.04±0.02	0.21±0.04	0.19±0.02	0.21±0	0.18±0.01	0.19±0.02	0.03±0.01	0.07±0.01
<b>Sample 4</b>	0.26±0.02	0.35±0.02	0.27±0.02	0.27±0.02	0.37±0.02	0.27±0.03	0.24±0.01	0.31±0.03	0.25±0.02
<b>Sample 5</b>	0.26±0.01	0.19±0.02	0.28±0	0.15±0.02	0.04±0.01	0.13±0.01	0.35±0.03	0.27±0.02	0.31±0
<b>Sample 6</b>	0.3±0.03	0.19±0.02	0.18±0.08	0.17±0.06	0.13±0.02	0.2±0.02	0.32±0.03	0.36±0.02	0.36±0.02

236 *Mechanical heterogeneity: Effect of region*

237 The mean value of the reduced modulus  $E_r$  was significantly higher in the cranial region  
238 ( $5.73 \pm 2.87$  MPa) compared to the caudal ( $2.18 \pm 2.26$  MPa,  $P < 0.001$ ) and the central ( $1.52 \pm 0.97$   
239 MPa,  $P < 0.001$ ) regions as displayed in Fig. 4A. There was no significant difference in stiffness  
240 mean values between the caudal and the central regions.

241 The mean value of the elastic fraction  $f$  was significantly higher in the cranial region  
242 ( $0.26 \pm 0.09$ ) compared to the caudal ( $0.22 \pm 0.07$ ,  $P < 0.001$ ) and the central ( $0.19 \pm 0.07$ ,  $P < 0.001$ )  
243 regions, the mean value of the elastic fraction  $f$  was also significantly higher in the caudal  
244 region compared to the central region ( $P < 0.005$ ) as displayed in Fig. 4B.



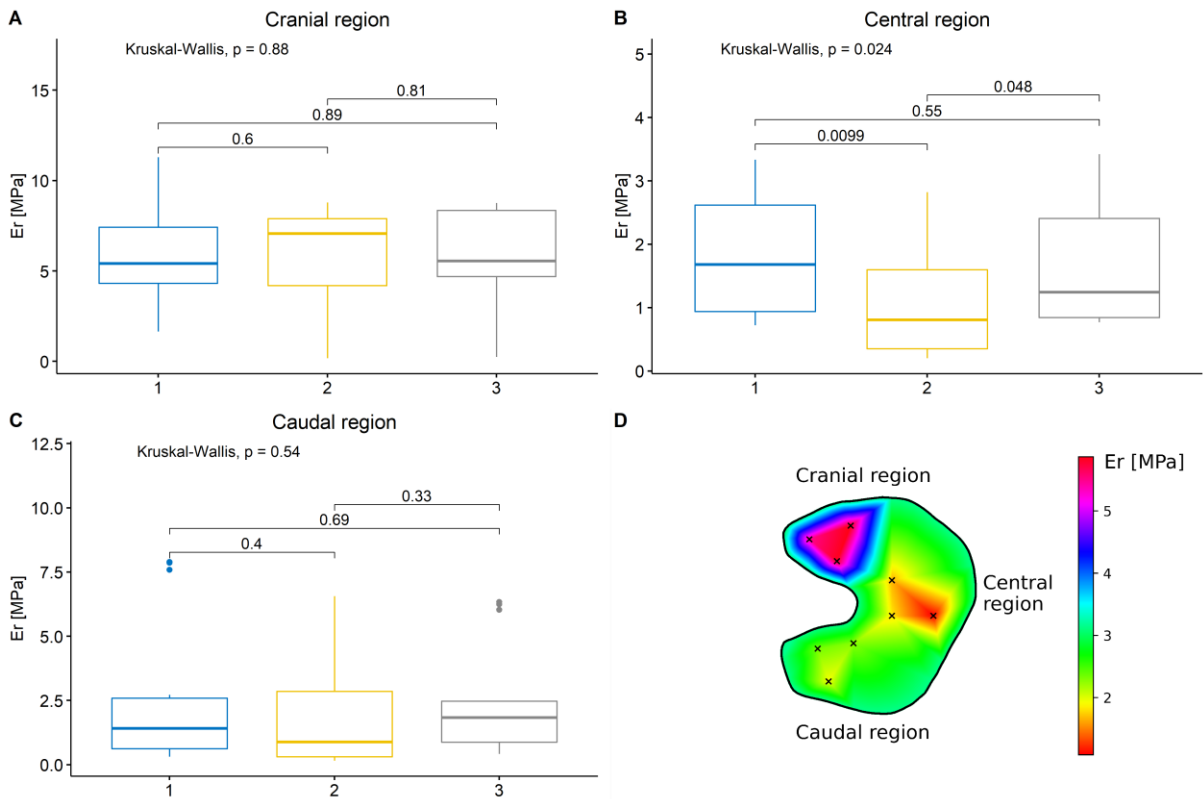
245  
246 Fig. 4. Effect of the region on (A) the reduced modulus  $E_r$  and (B) the elastic fraction  $f$ .

247

248 *Mechanical heterogeneity: Effect of the circumference*

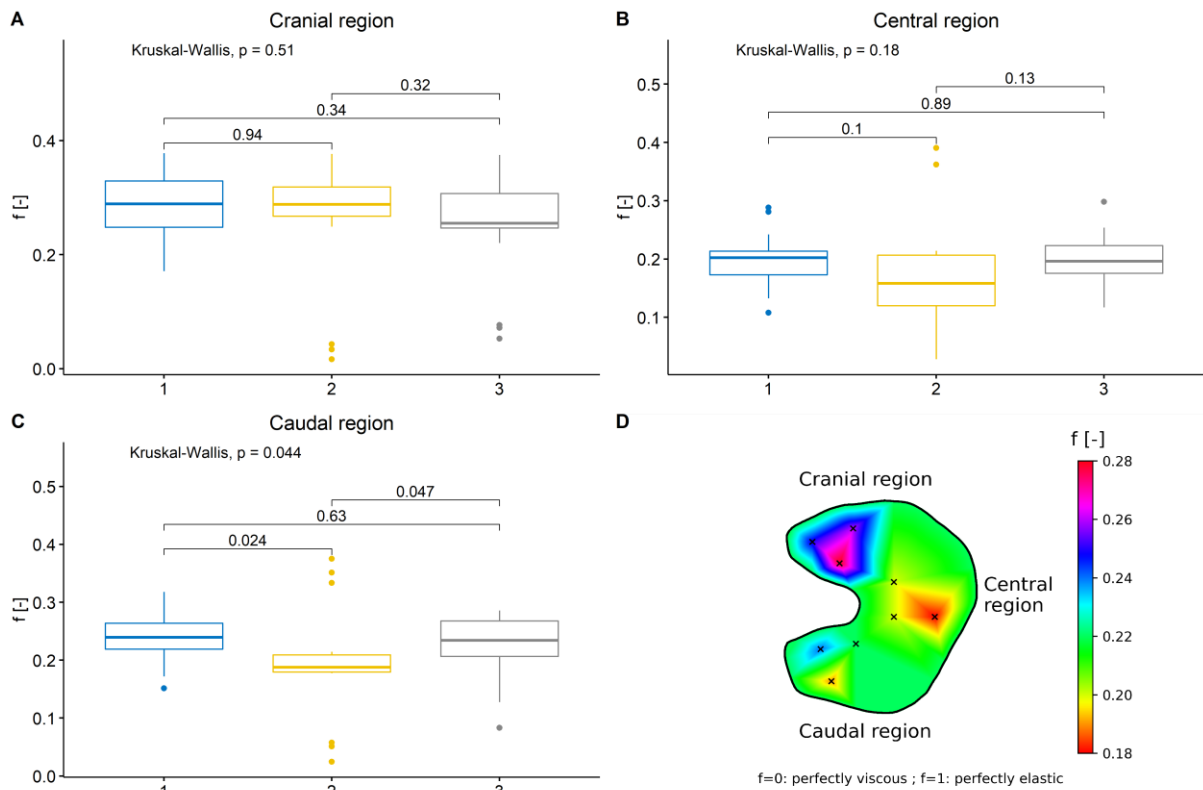
249 Within the cranial and the caudal regions, the mean value of the reduced modulus  $E_r$ ,  
250 was not different between the points 1, 2 and 3 (Fig. 5A and 5C). Within the central region, the  
251 mean value of the reduced modulus  $E_r$  was significantly lower in the periphery, for the point 2

252 (1.08±0.90 MPa), compared to the inner points 1 (1.82±0.92 MPa, P<0.01) and 3 (1.66±0.97  
 253 MPa, P<0.05) as displayed in Fig. 5B.



254  
 255 Fig. 5. Effect of the circumference on the reduced modulus  $E_r$  (A, B, C) and mapping of the  
 256 heterogeneity by linear interpolation onto the indented area (D) in each region.  
 257

258 Within the cranial and the central regions, the mean value of the elastic fraction  $f$  was  
 259 not different between the points 1, 2 and 3 (Fig. 6A and 6B). Within the caudal region, the mean  
 260 value of the elastic fraction  $f$  was significantly lower in the periphery, *i.e.* for the point 2  
 261 (0.19±0.09), compared to the inner points 1 (0.24±0.04, P<0.05) and 3 (0.22±0.05, P<0.05) as  
 262 displayed in Fig. 6C.



263

264 Fig. 6. Effect of the circumference on the elastic fraction  $f$  (A, B, C) and mapping of the  
 265 heterogeneity by linear interpolation onto the indented area (D) in each region.  
 266

267 An overall map of the reduced modulus and the elastic fraction are proposed (Fig. 5D  
 268 and Fig. 6D, respectively) to summarize the viscoelastic heterogeneity.

269

## 270 Discussion

271 We hypothesized that the mechanical behavior of the stifle menisci in healthy dogs is  
 272 heterogeneous and cannot be characterized and described as a whole elastic or viscoelastic  
 273 material. Our hypothesis was to consider regional variations and a radial dependency of the  
 274 micromechanical properties of the menisci. To our knowledge, this is the first report of  
 275 nanoindentation-relaxation in the stifle menisci in healthy (Beagle) dogs.

276 The results indicate significant micromechanical differences in the deep zone of the  
 277 medial menisci among regions and radial zones.

278 Firstly, the cranial region was significantly stiffer (higher  $E_r$ ) and less viscous (higher  $f$ ) than  
279 the central and caudal regions. The caudal region was stiffer (higher  $E_r$ , although not significant)  
280 and less viscous (higher  $f$ , significant) than the central region (Fig. 4).

281 Secondly, within the central region, the inner part was significantly stiffer (higher  $E_r$ ) than the  
282 periphery. Also, within the caudal region, the inner part was significantly less viscous (higher  
283  $f$ ) than the periphery (Fig. 5D and 6D).

284

285         Regarding regional variation of the micromechanical behavior, the comparison with the  
286 two previous studies on the canine meniscus biomechanics (Noone et al., 2002; Sweigart et al.,  
287 2004) is difficult due to the differences in methodology (creep indentation *versus* indentation  
288 tests), measurements (aggregate *versus* reduced modulus), sample preparation (cylindrical  
289 plugs *versus* trimmed menisci) and depth of indentation (on the surface *versus* in the deep zone  
290 Fig. 2B). Besides, neither the breed nor the weight, sex, age, radiographic and gross anatomic  
291 evaluations were specified. Here, all dogs were female beagles of the same age and of very  
292 similar weight, clinical, radiographic and post-mortem gross observation confirmed the  
293 “healthy” status of the joints. The knowledge of the breed is paramount since there is a large  
294 number of breeds with high risk of developmental orthopedic diseases (LaFond et al., 2002;  
295 Anderson et al., 2020). Other data such as age, sex, weight, body condition have to be  
296 mentioned as they are risks factors for canine osteoarthritis (Anderson et al., 2018), which could  
297 impair the “healthy” status of menisci, even in young dogs. Tellegen et al., 2019 showed a  
298 systematic difference in both healthy and osteoarthritic cartilage between dog breeds,  
299 accordingly, the chondrodystrophic status of the breed and the body conformation has to be  
300 considered. The Beagle, a chondrodystrophic breed, is the most commonly used breed in dog  
301 models of osteoarthritis (Dhollander et al., 2017), making the study of healthy meniscus in this  
302 breed important for joint diseases research.

303 Here, only the medial meniscus was investigated due to the high incidence of tears (bucket-  
304 handle lesions) in the caudal horn but it would be interesting to study the micromechanics of  
305 the lateral meniscus since there are differences in anatomy, fixation and kinematics between  
306 both the lateral and medial canine menisci (Park et al., 2018).

307

308         Regarding circumferential variations of the micromechanical properties, this has never  
309 been studied in the dog, and overall, data are lacking in respect to peripheral and inner regions.  
310 Our study adds another dimension to the knowledge of the regionally dependent properties of  
311 the menisci since, we observed that the inner part was significantly stiffer within the central  
312 region and significantly less viscous within the caudal region than the periphery (Fig. 5D and  
313 6D). Using dynamic mechanical analysis, Murphy et al., 2019 studied the viscoelastic variation  
314 between the inner and peripheral zones in the central region of bovine menisci. They showed  
315 that the inner zone displayed a higher average storage modulus (more elastic) than the  
316 periphery, though not significantly. Studies are needed to determine the origin of these  
317 differences and specially to investigate both collagen fibrils and fluid contents (Danso et al.,  
318 2015; Murphy et al., 2019).

319

320 The significant micromechanical differences in the deep zone of the medial menisci among  
321 regions and circumferential (radial) zones validated our hypothesis. The elastic fraction has  
322 seldom been used to study menisci mechanical properties, yet it allows the distinction between  
323 elastic and viscous behaviors, which is related to distinct structural elements and their geometry  
324 within the tissue. In the present study, the mean elastic fraction was strictly below 0.5 meaning  
325 a viscous rather than an elastic behavior similarly, as in the deep zone of healthy rabbits  
326 (Levillain et al., 2015), and in both the surface and deep zones of human menisci (Moyer et al.,  
327 2013, 2012). Although the parameters of soft biological tissues viscoelastic models (with Prony

328 series) are not yet linked to the microstructure component, this approach gives a better view of  
329 its micromechanical behavior.

330

### 331 **Conclusion**

332 Nanoindentation-relaxation testing showed significant regional and radial variations in  
333 micromechanical properties at one defined depth for both the stiffness and the elastic fraction,  
334 which impairs the use of an average elastic modulus to study the mechanical behavior of  
335 meniscus. Further developments are needed to understand the link between the microstructural  
336 arrangement of soft biological tissues components and their micromechanical behavior.

337

### 338 **Conflict of interest statement**

339 The authors declared no potential conflicts of interest with respect to the research,  
340 authorship, and/or publication of this article.

341

### 342 **Acknowledgements**

343 The authors wish to thank Dr. Aurélie Levillain as Ph.D. student during the study for  
344 her help in the experimental design, Dr. Catherine Bosser as engineer on the IVTV platform for  
345 her technical support, Dr. Claude Carozzo for his surgical expertise, Dr. Hélène Magoariec for  
346 her kind review of the paper and helpful discussions, the LTDS laboratory for providing a  
347 working space and the IVTV ANR-10-EQPX-06-01 for the financial support.

348

### 349 **References**

350 Anderson, K.L., O'Neill, D.G., Brodbelt, D.C., Church, D.B., Meeson, R.L., Sargan, D.,  
351 Summers, J.F., Zulch, H., Collins, L.M., 2018. Prevalence, duration and risk factors  
352 for appendicular osteoarthritis in a UK dog population under primary veterinary care.  
353 *Sci Rep* 8, 5641. <https://doi.org/10.1038/s41598-018-23940-z>

354 Anderson, K.L., Zulch, H., O'Neill, D.G., Meeson, R.L., Collins, L.M., 2020. Risk Factors  
355 for Canine Osteoarthritis and Its Predisposing Arthropathies: A Systematic Review.  
356 *Front Vet Sci* 7, 220. <https://doi.org/10.3389/fvets.2020.00220>

357 Arnoczky, S.P., Warren, R.F., 1983. The microvasculature of the meniscus and its response to  
358 injury. An experimental study in the dog. *Am J Sports Med* 11, 131–141.  
359 <https://doi.org/10.1177/036354658301100305>

360 Bennett, D., May, C., 1991. Meniscal damage associated with cruciate disease in the dog.  
361 *Journal of Small Animal Practice* 32, 111–117. <https://doi.org/10.1111/j.1748-5827.1991.tb00524.x>

362 Briggs, K.K., 2004. The Canine Meniscus: Injury and Treatment. *Compend Contin Educ Pract Vet* 26, 687–697.

363 Casale, S.A., McCarthy, R.J., 2009. Complications associated with lateral fabellotibial suture  
364 surgery for cranial cruciate ligament injury in dogs: 363 cases (1997-2005). *J Am Vet Med Assoc* 234, 229–235. <https://doi.org/10.2460/javma.234.2.229>

365 Case, J.B., Hulse, D., Kerwin, S.C., Peycke, L.E., 2008. Meniscal injury following initial  
366 cranial cruciate ligament stabilization surgery in 26 dogs (29 stifles). *Vet Comp Orthop Traumatol* 21, 365–367. <https://doi.org/10.3415/vcot-07-07-0070>

367 Charan, J., Kantharia, N.D., 2013. How to calculate sample size in animal studies? *J Pharmacol Pharmacother* 4, 303–306. <https://doi.org/10.4103/0976-500X.119726>

368 Clark, J.M., Norman, A.G., Kääh, M.J., Nötzli, H.P., 1999. The surface contour of articular  
369 cartilage in an intact, loaded joint. *J Anat* 195 ( Pt 1), 45–56.  
370 <https://doi.org/10.1046/j.1469-7580.1999.19510045.x>

371 Danso, E.K., Mäkelä, J.T.A., Tanska, P., Mononen, M.E., Honkanen, J.T.J., Jurvelin, J.S.,  
372 Töyräs, J., Julkunen, P., Korhonen, R.K., 2015. Characterization of site-specific  
373 biomechanical properties of human meniscus-Importance of collagen and fluid on  
374 mechanical nonlinearities. *J Biomech* 48, 1499–1507.  
375 <https://doi.org/10.1016/j.jbiomech.2015.01.048>

376 Dhollander, A., Malone, A., Price, J., Getgood, A., 2017. Determination of knee cartilage  
377 volume and surface area in beagle dogs: a pilot study. *J Exp Orthop* 4, 35.  
378 <https://doi.org/10.1186/s40634-017-0109-1>

379 Ebenstein, D.M., Kuo, A., Rodrigo, J.J., Reddi, A.H., Ries, M., Pruitt, L., 2004. A  
380 nanoindentation technique for functional evaluation of cartilage repair tissue. *Journal of Materials Research* 19, 27. <https://doi.org/10.1557/jmr.2004.19.1.273>

381 Fox, A.J.S., Wanivenhaus, F., Burge, A.J., Warren, R.F., Rodeo, S.A., 2015. The human  
382 meniscus: a review of anatomy, function, injury, and advances in treatment. *Clin Anat*  
383 28, 269–287. <https://doi.org/10.1002/ca.22456>

384 Huang, G., Lu, H., 2006. Measurement of Young's relaxation modulus using nanoindentation.  
385 *Mech Time-Depend Mater* 10, 229–243. <https://doi.org/10.1007/s11043-006-9020-3>

386 LaFond, E., Breur, G.J., Austin, C.C., 2002. Breed susceptibility for developmental  
387 orthopedic diseases in dogs. *J Am Anim Hosp Assoc* 38, 467–477.  
388 <https://doi.org/10.5326/0380467>

389 Levillain, A., Boulocher, C., Kaderli, S., Viguier, E., Hannouche, D., Hoc, T., Magoaric, H.,  
390 2015. Meniscal biomechanical alterations in an ACLT rabbit model of early  
391 osteoarthritis. *Osteoarthritis Cartilage* 23, 1186–1193.  
392 <https://doi.org/10.1016/j.joca.2015.02.022>

393 Levillain, A., Magoaric, H., Boulocher, C., Decambon, A., Viateau, V., Hoc, T., 2017.  
394 Viscoelastic properties of rabbit osteoarthritic menisci: A correlation with matrix  
395 alterations. *J Mech Behav Biomed Mater* 65, 1–10.  
396 <https://doi.org/10.1016/j.jmbbm.2016.08.015>

402

403 Makris, E.A., Hadidi, P., Athanasiou, K.A., 2011. The knee meniscus: structure-function,  
404 pathophysiology, current repair techniques, and prospects for regeneration.  
405 *Biomaterials* 32, 7411–7431. <https://doi.org/10.1016/j.biomaterials.2011.06.037>  
406 Messner, K., Gao, J., 1998. The menisci of the knee joint. Anatomical and functional  
407 characteristics, and a rationale for clinical treatment. *J Anat* 193 ( Pt 2), 161–178.  
408 <https://doi.org/10.1046/j.1469-7580.1998.19320161.x>  
409 Moyer, J.T., Abraham, A.C., Haut Donahue, T.L., 2012. NANOINDENTATION OF  
410 HUMAN MENISCAL SURFACES. *J Biomech* 45, 2230–2235.  
411 <https://doi.org/10.1016/j.jbiomech.2012.06.017>  
412 Moyer, J.T., Priest, R., Bouman, T., Abraham, A.C., Donahue, T.L.H., 2013. Indentation  
413 properties and glycosaminoglycan content of human menisci in the deep zone. *Acta*  
414 *Biomater* 9, 6624–6629. <https://doi.org/10.1016/j.actbio.2012.12.033>  
415 Murphy, C.A., Cunniffe, G.M., Garg, A.K., Collins, M.N., 2019. Regional dependency of  
416 bovine meniscus biomechanics on the internal structure and glycosaminoglycan  
417 content. *J Mech Behav Biomed Mater* 94, 186–192.  
418 <https://doi.org/10.1016/j.jmbbm.2019.02.020>  
419 Noone, T.J., Millis, D.L., Korvick, D.L., Athanasiou, K., Cook, J.L., Kuroki, K., Buonomo,  
420 F., 2002. Influence of canine recombinant somatotropin hormone on biomechanical  
421 and biochemical properties of the medial meniscus in stifles with altered stability. *Am*  
422 *J Vet Res* 63, 419–426. <https://doi.org/10.2460/ajvr.2002.63.419>  
423 Oliver, W.C., Pharr, G.M., 1992. An improved technique for determining hardness and elastic  
424 modulus using load and displacement sensing indentation experiments. *Journal of*  
425 *Materials Research* 7, 1564–1583. <https://doi.org/10.1557/JMR.1992.1564>  
426 Oyen, M., 2015. Nanoindentation of Hydrated Materials and Tissues.  
427 <https://doi.org/10/254456>  
428 Park, B.H., Banks, S.A., Pozzi, A., 2018. Quantifying meniscal kinematics in dogs. *J Orthop*  
429 *Res* 36, 1710–1716. <https://doi.org/10.1002/jor.23800>  
430 Pozzi, A., Kowaleski, M.P., Apelt, D., Meadows, C., Andrews, C.M., Johnson, K.A., 2006.  
431 Effect of medial meniscal release on tibial translation after tibial plateau leveling  
432 osteotomy. *Vet Surg* 35, 486–494. <https://doi.org/10.1111/j.1532-950X.2006.00180.x>  
433 Sweigart, M.A., Zhu, C.F., Burt, D.M., DeHoll, P.D., Agrawal, C.M., Clanton, T.O.,  
434 Athanasiou, K.A., 2004. Intraspecies and interspecies comparison of the compressive  
435 properties of the medial meniscus. *Ann Biomed Eng* 32, 1569–1579.  
436 <https://doi.org/10.1114/b:abme.0000049040.70767.5c>  
437 Tellegen, A.R., Dessing, A.J., Houben, K., Riemers, F.M., Creemers, L.B., Mastbergen, S.C.,  
438 Meij, B.P., Miranda-Bedate, A., Tryfonidou, M.A., 2019. Dog as a Model for  
439 Osteoarthritis: The FGF4 Retrogene Insertion May Matter. *J Orthop Res* 37, 2550–  
440 2560. <https://doi.org/10.1002/jor.24432>  
441 Witsberger, T.H., Villamil, J.A., Schultz, L.G., Hahn, A.W., Cook, J.L., 2008. Prevalence of  
442 and risk factors for hip dysplasia and cranial cruciate ligament deficiency in dogs. *J*  
443 *Am Vet Med Assoc* 232, 1818–1824. <https://doi.org/10.2460/javma.232.12.1818>  
444

